PairDropGS: Paired Dropout-Induced Consistency Regularization for Sparse-View Gaussian Splatting

Hantang Li, Qiang Zhu, Xiandong Meng, Xingtao Wang, Debin Zhao, and Xiaopeng Fan, *Senior Member, IEEE*

***Abstract*—Dropout-based sparse-view 3D Gaussian Splatting (3DGS) methods alleviate overfitting by randomly suppressing Gaussian primitives during training. Existing methods mainly focus on designing increasingly sophisticated dropout strategies, while they overlook the resulting inconsistencies among different dropped Gaussian subsets. This oversight often leads to unstable reconstruction and suboptimal Gaussian representation learning. In this paper, we revisit dropout-based sparse-view 3DGS from a consistency regularization perspective and propose PairDropGS, a Paired Dropout-induced Consistency Regularization framework for sparse-view Gaussian splatting. Specifically, PairDropGS first constructs a pair of the dropped Gaussian subsets from a shared Gaussian field and designs a low-frequency consistency regularization to constrain their low-frequency rendered structures. This design encourages the shared Gaussian field to preserve stable scene layout and coarse geometry under different random dropouts, while avoiding excessive constraints on ambiguous high-frequency details. Moreover, we introduce a progressive consistency scheduling strategy to gradually strengthen the consistency regularization during training for stability and robustness of reconstruction. Extensive experiments on widely-used sparse-view benchmarks demonstrate that PairDropGS achieves superior training stability, significantly outperforms existing dropout-based 3DGS methods in reconstruction quality, while exhibiting the simplicity and plug-and-play nature for improving dropout-based optimization.**

***Index Terms*—3D Gaussian splatting, sparse-view reconstruction, novel view synthesis, dropout regularization, consistency learning.**

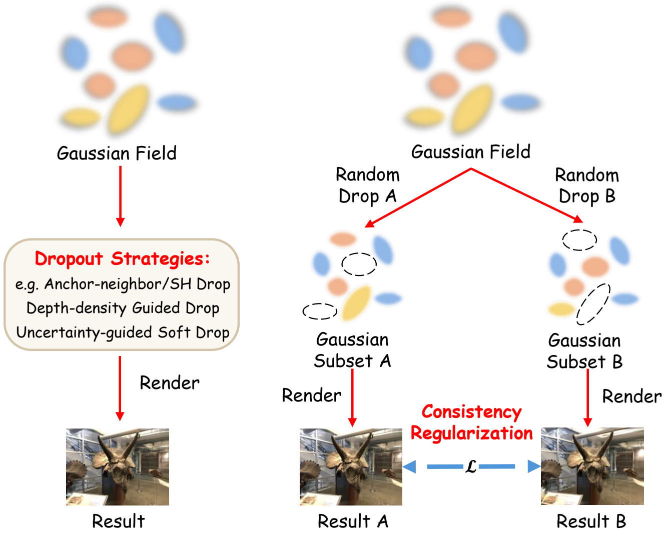

(a) Existing methods (b) PairDropGS

Fig. 1: **Comparison of existing dropout-based methods and PairDropGS.** (a) Existing dropout-based methods mainly design sophisticated dropout strategies for improving sparse-view reconstruction. (b) In contrast, PairDropGS constructs a pair of dropped Gaussian subsets from a shared Gaussian field and explicitly regularizes consistency of their rendered structures for stable and robust sparse-view reconstruction.

I. INTRODUCTION

Novel view synthesis under sparse-view settings remains a highly challenging problem due to severe overfitting and insufficient geometric constraints caused by limited input observations. Recently, 3D Gaussian Splatting (3DGS) [1] has emerged as a powerful representation for efficient and high-quality novel view synthesis [2]–[5]. Compared with implicit neural radiance fields [6]–[9], 3DGS achieves substantially faster optimization and real-time rendering by representing scenes as explicit Gaussian primitives. However, directly optimizing Gaussian primitives under sparse-view conditions often leads to unreliable scene representations, geometric ambiguity, and degraded rendering quality on unseen views. To alleviate these issues, many sparse-view reconstruction methods [8], [10]–[16] have been proposed, such as geometry-aware priors-guided methods [8], [11], [12], [15] and regularization-based methods [10], [14], [17]. Among them, recent dropout-based regularization methods [18]–[24] have demonstrated particularly promising performance by randomly suppressing Gaussian primitives during training to alleviate overfitting under sparse observations. These methods improve reconstruction quality mainly through carefully designed dropout strategies [20]–[23], such as geometry-aware Gaussian suppression [20], uncertainty-guided dropping [23], and structure-aware dropout regularization [21], [22]. Due to their competitive reconstruction quality, dropout-based methods have become a major direction for sparse-view Gaussian splatting.

However, existing dropout-based methods still face several key problems. **First**, sparse-view supervision offers limited observations and insufficient geometric constraints, making optimization much more sensitive to dropout-induced perturbations. Consequently, inconsistencies between different dropped Gaussian subsets can be significantly amplified during

---

Hantang Li is with the School of Computer Science, Harbin Institute of Technology, Shenzhen, China, and also with Pengcheng Laboratory, Shenzhen, China (e-mail: 25B951062@stu.hit.edu.cn). Qiang Zhu and Xiandong Meng are with the Smart Coding Institute, Pengcheng Laboratory, Shenzhen, China. Xingtao Wang, Debin Zhao and Xiaopeng Fan are with the School of Computer Science, Harbin Institute of Technology, Harbin, China.

Xiandong Meng and Xiaopeng Fan are corresponding authors (e-mail: mengxd@pcl.ac.cn, fxp@hit.edu.cn).

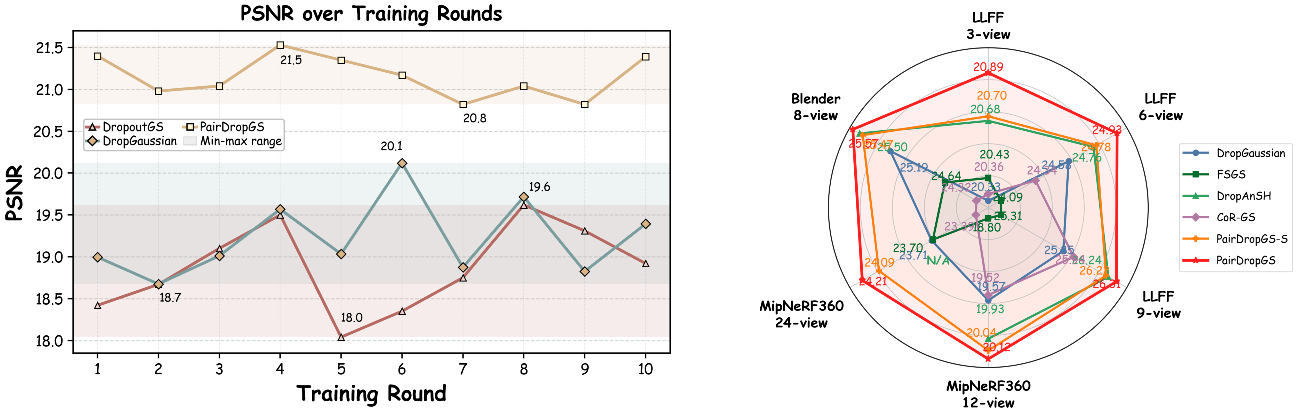

(a)

(b)

Fig. 2: **Stability and performance comparisons of existing methods and PairDropGS.** (a) PSNR variation across different training rounds on the LLFF 3-view *horns_00003* scene. Existing dropout-based methods show large performance fluctuations, while PairDropGS achieves more stable and higher reconstruction quality. (b) Overall PSNR comparison. PairDropGS significantly and consistently outperforms existing methods under different datasets and sparse-view settings. PairDropGS-S denotes a lightweight variant with a shortened training schedule to reduce the training cost.

training. As illustrated in Fig. 2(a), existing dropout-based methods [18], [19] exhibit noticeable fluctuations across different training rounds, leading to unstable Gaussian representation learning and inconsistent rendering quality. Several recent methods introduce increasingly sophisticated dropout strategies [20]–[23], such as depth-and density-aware dropping [20], uncertainty-guided masking [23], anchor-neighbor search with SH-specific dropout [22], as illustrated in Fig. 1(a). However, they increase model complexity, parameter sensitivity, and implementation cost by regularizing sparse-view optimization at the Gaussian primitive level, while still insufficiently addressing stochastic inconsistencies and robustness under sparse-view settings. **Second**, under limited observations, high-frequency details are often ambiguous and prone to overfitting [10], [16]. Current dropout-based strategies [19], [20], [24] fail to explicitly distinguish reliable structural cues from ambiguous high-frequency variations. Consequently, the learned Gaussian representation remains sensitive to stochastic perturbations in local textures or high-frequency regions, resulting in unstable training, inconsistent structures, and limited robustness. **Third**, existing methods usually employ fixed or predefined dropout strategies throughout training. They often either over-constrain early optimization or under-constrain stochastic inconsistency in later optimization, making the final reconstruction less stable to training randomness.

To address the above issues, we revisit and redesign the dropout-based framework. **First**, we revisit dropout-based sparse-view Gaussian splatting from a consistency regularization perspective rather than increasingly complicated dropout strategies. Specifically, we propose a simple yet effective **Pair**ed **Drop**out-induced Consistency Regularization framework for sparse-view **G**aussian **S**platting, denoted as **PairDropGS**. As illustrated in Fig. 1, PairDropGS constructs a pair of dropped Gaussian subsets from the same shared Gaussian field under the same training view. By explicitly constraining the structural responses rendered from the paired Gaussian subsets, our framework regularizes the shared Gaussian representation to remain stable under different dropout masks, improving the stability and robustness of sparse-view reconstruction. **Furthermore**, we design a low-frequency consistency regularization mechanism that aligns the paired Gaussian subsets in the low-frequency subspace rather than directly enforcing consistency of global rendered results. This design encourages different dropped Gaussian subsets to preserve consistent scene layout and coarse geometry, while still maintaining sufficient flexibility for ambiguous high-frequency details and texture variations. **Finally**, we introduce a progressive consistency scheduling strategy that gradually increases the reliability of consistency regularization throughout training, which preserves sufficient optimization flexibility during early structure formation, while strengthening consistency constraints in later stages to suppress accumulated inconsistency, overfitting, and structural drift.

The main contributions of our work are as follows:

- We revisit dropout-based sparse-view Gaussian splatting from a consistency regularization perspective and propose **PairDropGS**, a simple yet effective **Pair**ed **Drop**out-induced consistency regularization **G**aussian **S**platting framework that improves training stability, reconstruction quality and robustness without introducing complex dropout strategies or external priors.
- We design a **low-frequency consistency regularization** mechanism that explicitly aligns the reliable structural responses rendered from paired Gaussian subsets, improving scene stability while avoiding excessive constraints on ambiguous high-frequency details.
- We propose a **progressive consistency scheduling** strategy that adaptively strengthens subset consistency regularization during training to suppress accumulated inconsistency for improving optimization robustness.

Extensive experiments on three challenging sparse-view benchmarks demonstrate that PairDropGS consistently improves training stability, reconstruction quality and robustness over existing dropout-based methods while exhibiting the simplicity and plug-and-play nature for improving dropout-based Gaussian splatting, as illustrated in Fig. 2(b).

II. RELATED WORK

A. Novel View Synthesis with 3D Gaussian Splatting

Novel view synthesis (NVS) aims to synthesize photo-realistic images from unseen viewpoints given a set of input observations. Traditional image-based rendering and multi-view reconstruction methods rely on explicit geometry estimation, image warping, or multi-view stereo, but often degrade when observations are sparse. Neural Radiance Fields (NeRF) [25] achieve high-quality rendering by modeling scenes as continuous volumetric radiance fields. Subsequent works further improve NeRF from different aspects, including anti-aliasing [6], camera pose refinement [26], accelerated training [27], prior-guided synthesis [28], and generalizable sparse-input reconstruction [29]–[31]. However, NeRF-based methods usually require expensive ray sampling and network evaluation.

Recently, 3D Gaussian Splatting (3DGS) [1] has emerged as an efficient representation for real-time rendering by using explicit anisotropic Gaussian primitives. Many follow-up works improve 3DGS through anti-aliasing [32], structured representations [33], progressive Gaussian propagation [34], adaptive rendering enhancement [5], [35], multi-scale modeling [36], and sparse-view Gaussian prediction [37]. Despite these advances, 3DGS still relies on sufficient multi-view observations and suffers from geometric ambiguity, floaters, and overfitting under sparse-view settings.

B. Sparse-view Novel View Synthesis

Sparse-view NVS is inherently ill-posed due to limited observations and insufficient geometric constraints. Existing methods can be broadly grouped into three directions. First, geometry-aware methods introduce additional priors to reduce reconstruction ambiguity. For example, RegNeRF [8] and SparseNeRF [11] regularize NeRF training with geometry or depth priors, while DNGaussian [12], DRGS [38], SparseGS [39], NexusGS [15], and D^{2}GS [20] exploit depth, epipolar, or density cues to guide sparse-view Gaussian optimization. Second, regularization-based methods improve generalization by constraining the optimization process. FreeNeRF [10] and DWTGS [16] study frequency regularization, CoR-GS [14] introduces co-regularization and SE-GS [17] improves robustness through self-ensembling. Third, Gaussian refinement methods improve sparse-view rendering by enhancing primitive distribution or representation ability, such as FSGS [13], GaussianPro [34], ScaffoldGS [33], MSA-Splatting [36], and generative sparse-view Gaussian splatting [40]. Although these methods improve sparse-view reconstruction quality, many of them rely on additional priors, auxiliary modules, or complex optimization strategies.

C. Dropout-based Sparse-view Reconstruction

Dropout-based methods have recently shown strong potential for sparse-view Gaussian splatting by randomly suppressing Gaussian primitives during training. DropoutGS [18] introduces random dropout regularization to alleviate sparse-view overfitting, while DropGaussian [19] shows that randomly removing Gaussians can increase the visibility and gradients of non-dropped primitives. However, simple random dropout may be weakened by the neighborhood compensation effect, where nearby Gaussians compensate for dropped primitives [22].To strengthen dropout regularization, recent methods design more structure strategies, i.e., determining which Gaussians to drop and how to suppress unreliable Gaussian primitives. D^{2}GS [20] uses depth-and-density guided suppression, DropAnSH-GS [22] proposes anchor-neighbor dropout and SH-specific dropout, UGOD [23] performs uncertainty-guided soft dropout, and DOC-GS [21] explores reliability-oriented dropout and pruning. Co-Adaptation [24] further analyzes Gaussian entanglement through random Gaussian subset rendering. Although effective, these methods mainly focus on designing stronger dropout policies, such as what to drop and how to drop.

In contrast, PairDropGS shifts the focus from dropout strategy design to the stochastic behavior of dropout-based optimization itself. Instead of introducing more complex dropping rules, we explicitly regularize the consistency of the structural responses rendered from paired dropped Gaussian subsets, leading to more reliable Gaussian representation learning under sparse supervision.

III. PRELIMINARIES

A. 3D Gaussian Splatting

3D Gaussian Splatting (3DGS) represents a scene as a set of anisotropic Gaussian primitives $\mathcal{G} = \{G_i\}_{i=1}^{N}$, where N is the number of Gaussians. Each Gaussian G_i is associated with a mean $\mu_i \in R^3$, a covariance matrix $\Sigma_i \in R^{3\times3}$, a color term c_i, and an opacity parameter $\alpha_i \in [0, 1]$. For efficient optimization, the covariance is commonly parameterized by scaling and rotation components. Given a camera view v, the Gaussians are projected onto the image plane and ordered by depth along each viewing ray. The final color C at pixel u is computed through alpha compositing over all contributing Gaussians:

$$C(u) = \sum_i c_i \alpha_i \prod_{j<i} (1 - \alpha_j), \tag{1}$$

where the product term $\prod_{j<i}(1 - \alpha_j)$ represents the accumulated transmittance of Gaussians in front of the i-th one. Compared with implicit neural rendering, 3DGS enables substantially faster optimization and real-time rendering while maintaining competitive reconstruction quality.

B. Dropout-based Optimization

To alleviate sparse-view overfitting, dropout-based methods introduce stochastic regularization by randomly deactivating a subset of Gaussian primitives during training. Formally,

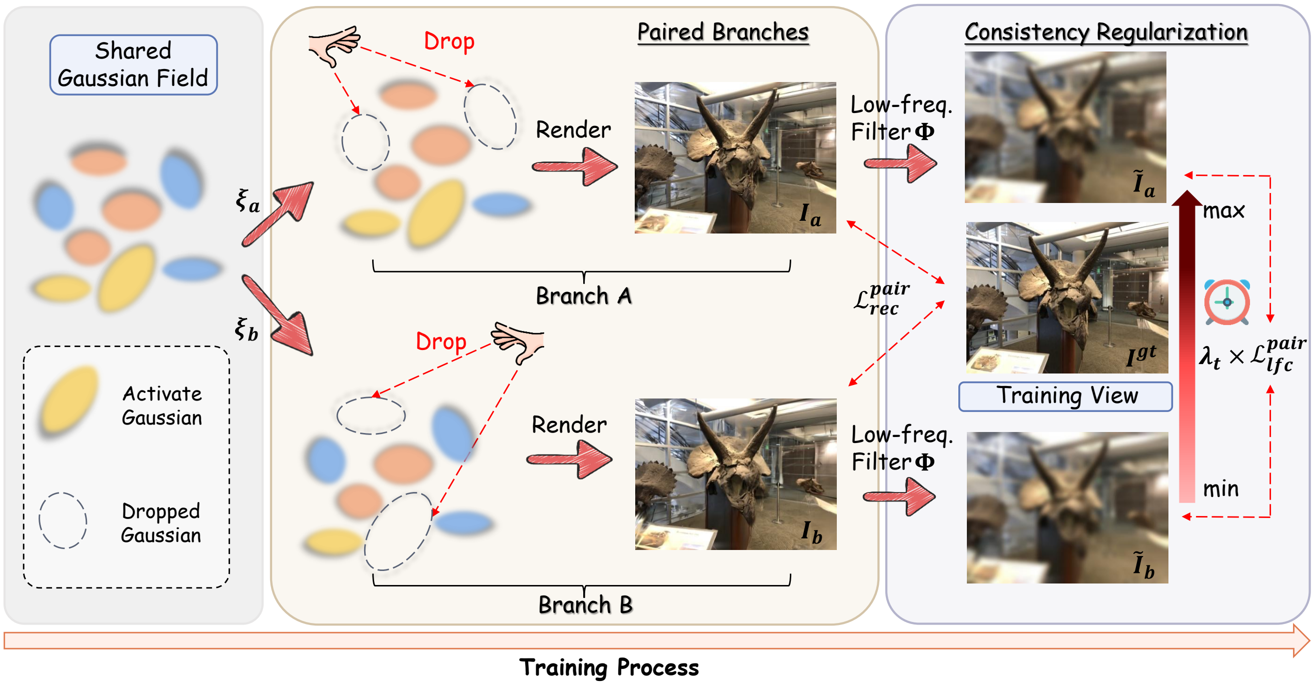

Fig. 3: **Overview of PairDropGS.** Starting from a shared Gaussian field, PairDropGS constructs two independently dropped Gaussian subsets under the same training view during training, forming paired branches. Both branches are supervised by the same ground-truth observation through two-branch reconstruction loss. To stabilize the structural responses rendered from different dropped subsets, the rendered images are processed by a low-frequency filter and constrained by low-frequency consistency regularization. A progressive consistency scheduling strategy is further adopted to gradually strengthen this constraint throughout training, improving the robustness of sparse-view Gaussian representation learning.

a binary dropout mask M is sampled to select the active Gaussians, and the rendered image is written as

$$I = \mathcal{R}(\mathcal{G} \odot M, v), \tag{2}$$

where $\odot$ denotes mask-based Gaussian subset selection, and $\mathcal{R}(\cdot)$ denotes the differentiable Gaussian rasterization process. Although such dropout regularization encourages the model to learn from different Gaussian subsets under limited observations, the varying active subsets may produce inconsistent structural responses. This inconsistency can introduce instability into Gaussian representation learning, especially when sparse-view photometric supervision is insufficient.

IV. METHOD

PairDropGS follows the standard SfM-initialized Gaussian splatting pipeline [19]–[21], [24] and proposes a paired dropout-induced consistency regularization framework for robust sparse-view reconstruction. As illustrated in Fig. 3, PairDropGS constructs a pair of dropped Gaussian subsets from the same shared Gaussian field under the same training view. The paired branches are jointly optimized by paired reconstruction supervision and further regularized by low-frequency consistency constraints with progressive consistency scheduling, thereby improving the stability and robustness of sparse-view Gaussian representation learning.

A. *PairDropGS Framework*

Existing dropout-based methods usually render only one randomly dropped Gaussian subset during each training iteration. However, under sparse-view settings, different dropped Gaussian subsets may produce inconsistent structural responses even when they originate from the same Gaussian field. This inconsistency may gradually accumulate during optimization, leading to unstable reconstruction behaviors and structural drift.

To alleviate this issue, PairDropGS explicitly models the consistency between different dropped Gaussian subsets during training. Specifically, instead of relying on a single dropped Gaussian subset, we construct a pair of dropped Gaussian subsets from the same shared Gaussian field $\mathcal{G}$ under the same training view v. The corresponding rendered images are denoted as I_a and I_b:

$$I_a = \mathcal{R}(\mathcal{G}; \xi_a, v), \qquad I_b = \mathcal{R}(\mathcal{G}; \xi_b, v), \tag{3}$$

where $\mathcal{R}(\cdot)$ denotes the differentiable Gaussian rasterization process, and ξ_a, ξ_b denote two independently sampled dropout masks. Although both branches share the same Gaussian representation $\mathcal{G}$ and the same training view v, different dropout masks activate different Gaussian subsets during rendering.

Both branches are supervised using the same ground-truth image I^{gt}. Following the standard 3DGS photometric supervision, the reconstruction loss $\mathcal{L}_{rgb}$ is defined as

$$\mathcal{L}_{rgb}(I, I^{gt}) = \mathcal{L}_{L_1}(I, I^{gt}) + \lambda_{d\text{-}ssim}\left(1 - \mathrm{SSIM}(I, I^{gt})\right), \tag{4}$$

where $\mathcal{L}_{L_1}$ denotes the pixel-wise L_1 loss, $\mathrm{SSIM}(\cdot)$ denotes the structural similarity index, and $\lambda_{d\text{-}ssim}$ balances the two terms. The two-branch reconstruction loss is then written as:

$$\mathcal{L}_{rec}^{pair} = \mathcal{L}_{rgb}(I_a, I^{gt}) + \beta\,\mathcal{L}_{rgb}(I_b, I^{gt}), \tag{5}$$

where β controls the reconstruction weight of the auxiliary branch. This paired optimization formulation allows the shared Gaussian field to learn more stable structural responses under different dropped Gaussian subsets while preserving the regularization effect of dropout-based optimization.

B. Low-Frequency Consistency Regularization

Although paired Gaussian subsets improve the diversity of stochastic supervision, directly constraining rendered images in the global rendered results may undesirably suppress necessary flexibility under sparse-view settings. In particular, sparse-view supervision usually provides weak constraints on fine details [16]. High-frequency components often admit multiple plausible solutions under sparse-view supervision, whereas low-frequency components usually provide more reliable cues for scene layout, coarse geometry, and global appearance [10], [16].

Based on this fact, PairDropGS regularizes the consistency between paired Gaussian subsets by matching their low-pass filtered renderings instead of directly enforcing global rendered image consistency. Specifically, we first apply a low-pass filtering operator $\Phi(\cdot)$ to the rendered images:

$$\tilde{I}_a = \Phi(I_a), \qquad \tilde{I}_b = \Phi(I_b), \tag{6}$$

where $\tilde{I}_a$ and $\tilde{I}_b$ denote the low-pass filtered renderings of the two branches, and $\Phi(\cdot)$ is implemented using Gaussian blur in practice.

To stabilize optimization, we further adopt an asymmetric consistency formulation with a stop-gradient operator:

$$\mathcal{L}_{lfc}^{pair} = \left\| \tilde{I}_a - \mathrm{sg}(\tilde{I}_b) \right\|_1, \tag{7}$$

where $\mathcal{L}_{lfc}^{pair}$ denotes the low-frequency consistency loss, and $\mathrm{sg}(\cdot)$ denotes the stop-gradient operator.

By constraining the low-frequency renderings produced from paired Gaussian subsets, PairDropGS encourages the shared Gaussian field to preserve stable scene layout and coarse geometry under different dropout masks while avoiding excessive constraints on ambiguous high-frequency details.

C. Progressive Consistency Scheduling

The influence of dropout-induced inconsistency is not uniform throughout training. During the early phase of optimization, the Gaussian field is still under-constrained and requires sufficient flexibility to fit sparse observations and establish reasonable scene structures. Applying strong consistency constraints too early may undesirably restrict the optimization space and hinder the formation of plausible geometry. As optimization proceeds, sparse-view reconstruction becomes increasingly sensitive to dropout-induced perturbations and overfitting effects [19], [20]. The discrepancy between different dropped Gaussian subsets may gradually accumulate into structural drift and unstable reconstruction behaviors, which is also related to the co-adaptation phenomenon observed in sparse-view Gaussian splatting [24]. Therefore, stronger consistency regularization becomes increasingly important during later optimization.

Motivated by this stage-dependent behavior, PairDropGS progressively strengthens low-frequency consistency regularization during training. Specifically, the consistency weight λ_t is defined as:

$$\lambda_t = \lambda_{\max} \cdot \min\left(1, \frac{t}{T_{warm}}\right), \tag{8}$$

where t denotes the current training iteration, $\lambda_{\max}$ is the maximum consistency weight, and T_{warm} controls the warm-up length. The overall loss $\mathcal{L}$ is then written as:

$$\mathcal{L} = \mathcal{L}_{rec}^{pair} + \lambda_t \mathcal{L}_{lfc}^{pair}. \tag{9}$$

This progressive design allows the model to first establish a reasonable reconstruction under sparse-view supervision and then gradually enforce cross-branch low-frequency consistency, thereby gradually improving reconstruction quality and training stability.

D. Discussion

PairDropGS does not rely on external priors, auxiliary networks, or increasingly complicated dropout strategies. Instead, it focuses on improving the robustness of dropout-based optimization by stabilizing the structural responses rendered from different dropped Gaussian subsets using simple dropout and low-frequency filtering operation. These designs enable more reliable sparse-view Gaussian representation learning while preserving the simplicity for improving dropout-based methods. We believe this work may serve as a strong, extensible and generalizable baseline for future sparse-view Gaussian splatting research.

V. EXPERIMENTS

A. Implementation Details

Training Details. In this work, a PairDropGS model and its lightweight model, i.e., PairDropGS-S, are proposed for the sparse-view Gaussian Splatting. PairDropGS employs the following hyperparameters and configurations: $\lambda_{d\text{-}ssim} = 0.2$, $\lambda_{\max} = 0.05$, $T_{warm} = 7000$, and the auxiliary branch reconstruction weight $\beta = 0.25$. The consistency weight is linearly warmed up during the first T_{warm} iterations. The low-pass filtering operator is implemented using Gaussian blur with kernel size 11 and standard deviation $\sigma = 3.0$. Following previous works [19], [22], the total number of iterations is 10000. PairDropGS-S is associated with a shortened training schedule to reduce the training cost introduced by paired branches, its total number of iterations is 5000 and $T_{warm} = 4000$, all other settings are unchanged. Our implementation is built upon DropGaussian [19], the dropout strategy and all other settings

TABLE I: Quantitative comparison on the LLFF dataset under sparse-view settings. The best and second-best results are shown in bold and underlined, respectively.

Category	Method	3-view			6-view			9-view		
		PSNR↑	SSIM↑	LPIPS↓	PSNR↑	SSIM↑	LPIPS↓	PSNR↑	SSIM↑	LPIPS↓
NeRF-based	Mip-NeRF [6]	16.11	0.401	0.460	22.91	0.756	0.213	24.88	0.826	0.170
	DietNeRF [41]	14.94	0.370	0.496	21.75	0.717	0.248	24.28	0.801	0.183
	RegNeRF [8]	19.08	0.587	0.336	23.10	0.760	0.206	24.86	0.820	0.161
	FreeNeRF [10]	19.63	0.612	0.308	23.73	0.779	0.195	25.13	0.827	0.160
	SparseNeRF [11]	19.86	0.624	0.328	–	–	–	–	–	–
3DGS-based	3DGS [1]	19.17	0.646	0.268	23.74	0.807	0.162	25.44	0.860	0.096
	DNGaussian [12]	19.12	0.591	0.294	22.18	0.755	0.198	23.17	0.788	0.180
	FSGS [13]	20.43	0.682	0.248	24.09	0.823	0.145	25.31	0.860	0.122
	CoR-GS [14]	20.36	0.710	0.202	24.34	0.831	0.122	25.94	0.872	0.088
	DropoutGS [18]	19.39	0.632	0.279	24.02	0.816	0.144	25.13	0.869	0.099
	DropGaussian [19]	20.33	0.709	0.201	24.58	0.830	0.125	25.85	0.864	0.093
	DropAnSH-GS [22]	20.68	0.724	0.194	24.76	0.837	0.116	26.24	0.875	0.088
	PairDropGS-S (Ours)	20.70	0.729	0.191	24.78	0.833	0.117	26.22	0.879	0.092
	PairDropGS (Ours)	**20.89**	**0.740**	**0.182**	**24.93**	**0.841**	**0.114**	**26.31**	**0.880**	**0.087**

TABLE II: Quantitative comparison on the MipNeRF-360 dataset under sparse-view settings. The best and second-best results are shown in bold and underlined, respectively.

Method	12-view			24-view		
	PSNR↑	SSIM↑	LPIPS↓	PSNR↑	SSIM↑	LPIPS↓
3DGS [1]	18.52	0.523	0.415	22.80	0.708	0.276
FSGS [13]	18.80	0.531	0.418	23.70	0.745	0.230
CoR-GS [14]	19.52	0.558	0.418	23.39	0.727	0.271
DropGaussian [19]	19.57	0.562	0.360	23.71	0.752	0.227
NexusGS [15]	–	–	–	23.86	0.753	**0.206**
DropAnSH-GS [22]	19.93	0.576	0.362	–	–	–
PairDropGS-S (Ours)	20.04	0.577	0.364	24.09	0.751	0.217
PairDropGS (Ours)	**20.12**	**0.585**	**0.357**	**24.21**	**0.762**	0.215

of our methods follow this work. Following a previous sparse-view reconstruction method [22], we report the average results over three independent runs. All experiments are conducted on a single NVIDIA A800 GPU.

Datasets and Metrics. Following previous sparse-view reconstruction methods [19], [22], we evaluate our methods on three widely-used benchmarks: two real-world datasets, i.e., LLFF [42] and MipNeRF-360 [7], and one synthetic dataset, i.e., Blender [25]. Following previous works [11], [19], 3, 6, and 9 input views for LLFF, 12 and 24 input views for MipNeRF-360, and 8 input views for Blender. Consistent with prior works [10], [11], [19], the standard sparse-view data splits and downsampling settings are employed. Additionally, we employ three evaluation metrics for evaluating the rendering quality: Peak Signal-to-Noise Ratio (PSNR), Structural Similarity Index (SSIM), and Learned Perceptual Image Patch Similarity (LPIPS). To evaluate the training efficiency of methods, we adopt the training time to measure them.

State-of-the-art Methods. We compare our methods with some representative NeRF-based methods, including Mip-NeRF [6], DietNeRF [41], RegNeRF [8], FreeNeRF [10], and SparseNeRF [11], as well as some 3DGS-based methods, including vanilla 3DGS [1], DNGaussian [12], FSGS [13], CoR-GS [14], and NexusGS [15]. Since our methods are designed for dropout-based sparse-view reconstruction, we pay particular attention to comparisons with existing dropout-based methods, such as DropoutGS [18], DropGaussian [19] and DropAnSH-GS [22].

TABLE III: Quantitative comparison on the Blender dataset under the sparse-view setting. The best and second-best results are shown in bold and underlined, respectively.

Method	PSNR↑	SSIM↑	LPIPS↓
3DGS [1]	21.56	0.847	0.130
DNGaussian [12]	24.31	0.886	0.088
NexusGS [15]	24.37	0.893	0.087
FSGS [13]	24.64	0.895	0.095
CoR-GS [14]	24.32	0.892	**0.084**
DropGaussian [19]	25.19	0.890	0.090
DropAnSH-GS [22]	25.50	0.891	0.088
PairDropGS-S (Ours)	25.47	0.890	0.088
PairDropGS (Ours)	**25.57**	**0.897**	0.086

B. Quantitative Comparison

We quantitatively evaluate our PairDropGS and PairDropGS-S against various NeRF-based and 3DGS-based methods on three datasets, i.e., the LLFF [42], MipNeRF-360 [7], and Blender [25], under different sparse-view settings. The corresponding results are reported in Tab. I, Tab. II, and Tab. III, respectively.

On the LLFF dataset, our PairDropGS achieves 20.89 dB in terms of PSNR under the highly restrictive 3-view setting, significantly outperforming the original 3DGS baseline by 1.72 dB and also surpassing recent state-of-the-art 3DGS-based methods, i.e., DropAnSH-GS [22] by 0.21 dB PSNR. As the number of input views increases, PairDropGS continues to demonstrate superior performance under both 6-view and 9-view settings. Similar improvements are also observed on the MipNeRF-360 and Blender datasets, where our PairDropGS

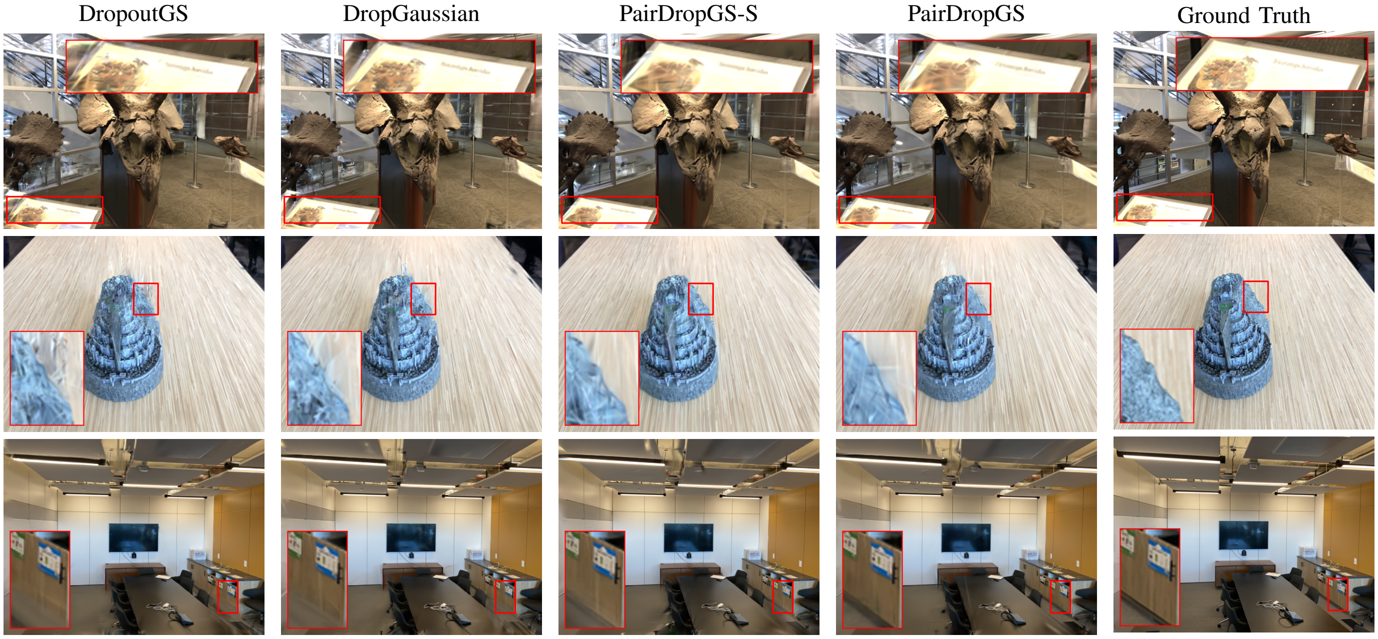

Fig. 4: Qualitative comparison of two sparse-view methods with our methods on the LLFF dataset under 3-view settings.

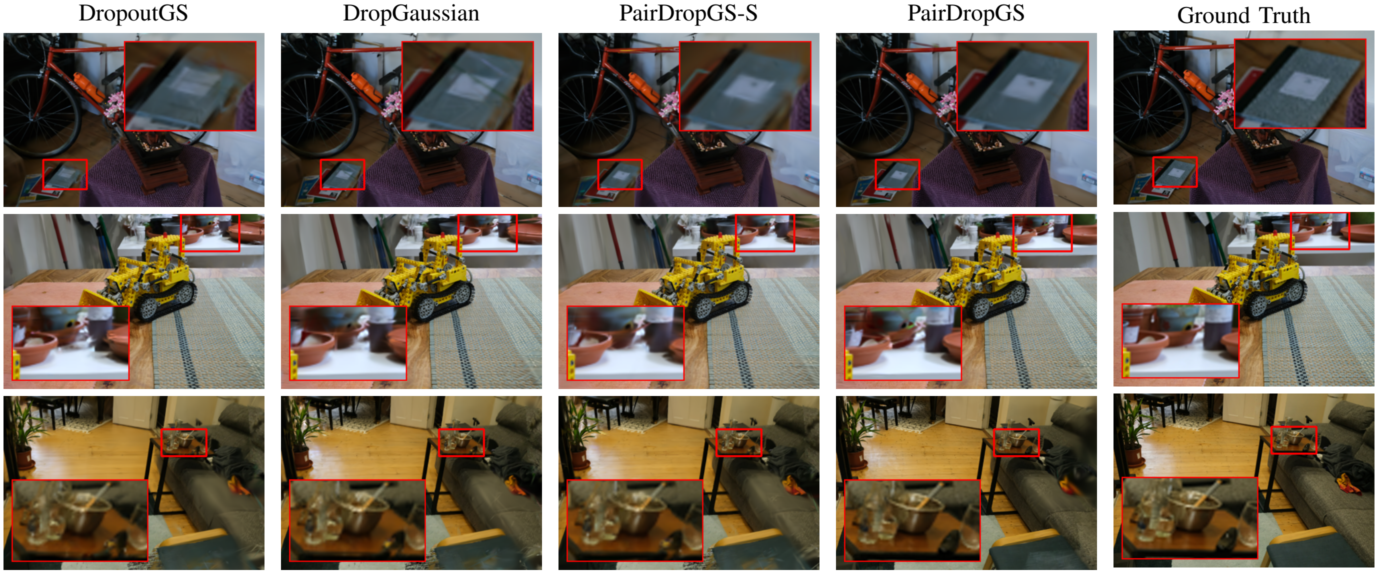

Fig. 5: Qualitative comparison of two sparse-view methods with our methods on the MipNeRF-360 dataset under 12-view settings.

consistently achieves competitive or best results across PSNR, SSIM, and LPIPS. Notably, PairDropGS-S, the lightweight variant with a shortened training schedule, still achieves performance comparable to or even better than existing state-of-the-art methods.

These results validate the effectiveness of PairDropGS. By explicitly constraining the structural responses rendered from paired dropped Gaussian subsets during training, PairDropGS mitigates the instability caused by dropout-based optimization and encourages the Gaussian field to learn more reliable scene representations under sparse-view supervision. Moreover, the consistent improvements across different datasets and sparsity levels demonstrate that PairDropGS generalizes well while preserving the simplicity, plug-and-play nature, and robustness of dropout-based Gaussian splatting.

C. Qualitative Comparison

As illustrated in Fig. 4, Fig. 5, and Fig. 6, we present qualitative comparisons with two representative dropout-based sparse-view methods, i.e., DropoutGS [18] and DropGaussian [19]. Regions with noticeable differences are highlighted by red bounding boxes. Existing dropout-based methods may still suffer from unstable structural responses under different dropped Gaussian subsets, leading to blurred boundaries, local inconsistencies, or over-smoothed appearances. Although DropoutGS and DropGaussian improve reconstruc-

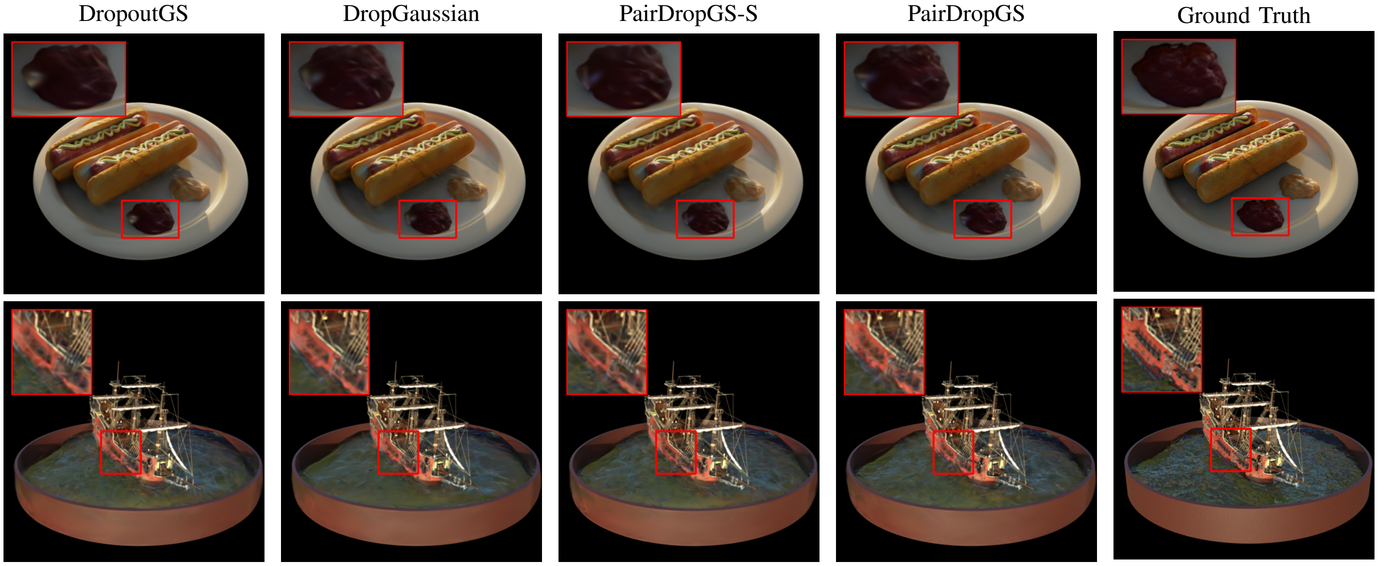

Fig. 6: Qualitative comparison of two sparse-view methods with our methods on the Blender dataset under 8-view settings.

TABLE IV: Per-scene fluctuation on the LLFF dataset under 3-view settings. We report mean ± standard deviation over 10 random seeds.

Method	Fern			Flower			Fortress		
	PSNR↑	SSIM↑	LPIPS↓	PSNR↑	SSIM↑	LPIPS↓	PSNR↑	SSIM↑	LPIPS↓
DropoutGS	21.55±0.186	0.647±0.0088	0.285±0.0097	19.20±0.273	0.571±0.0106	0.308±0.0103	22.50±0.427	0.684±0.0126	0.261±0.0090
DropGaussian	22.42±0.254	0.724±0.0094	0.202±0.0081	20.02±0.399	0.654±0.0112	0.221±0.0098	23.38±0.152	0.756±0.0091	0.182±0.0081
PairDropGS	**23.00±0.082**	**0.765±0.0062**	**0.185±0.0063**	**20.66±0.101**	**0.677±0.0065**	**0.200±0.0079**	**24.05±0.118**	**0.795±0.0055**	**0.166±0.0048**

Method	Horns			Leaves			Orchids		
	PSNR↑	SSIM↑	LPIPS↓	PSNR↑	SSIM↑	LPIPS↓	PSNR↑	SSIM↑	LPIPS↓
DropoutGS	17.97±0.326	0.599±0.0105	0.334±0.0103	16.30±0.242	0.581±0.0091	0.290±0.0097	14.90±0.395	0.481±0.0141	0.316±0.0115
DropGaussian	18.92±0.266	0.670±0.0098	0.249±0.0102	17.18±0.266	0.660±0.0094	0.209±0.0094	15.52±0.286	0.558±0.0140	0.232±0.0103
PairDropGS	**19.62±0.115**	**0.702±0.0062**	**0.224±0.0078**	**17.74±0.089**	**0.688±0.0049**	**0.191±0.0062**	**16.25±0.160**	**0.581±0.0092**	**0.206±0.0091**

Method	Room			Trex			Average		
	PSNR↑	SSIM↑	LPIPS↓	PSNR↑	SSIM↑	LPIPS↓	PSNR↑	SSIM↑	LPIPS↓
DropoutGS	21.13±0.262	0.777±0.0146	0.234±0.0094	21.33±0.254	0.679±0.0120	0.213±0.0082	19.36±0.1965	0.626±0.0029	0.279±0.0023
DropGaussian	22.17±0.325	0.840±0.0110	0.169±0.0091	**23.43±0.161**	0.812±0.0105	0.156±0.0083	20.38±0.1724	0.710±0.0024	0.200±0.0022
PairDropGS	**22.81±0.142**	**0.860±0.0064**	**0.144±0.0055**	22.99±0.112	**0.840±0.0048**	**0.138±0.0051**	**20.91±0.0726**	**0.739±0.0011**	**0.182±0.0012**

tion quality through dropout-based regularization, they do not explicitly stabilize the structural responses rendered from different dropped subsets during optimization. By contrast, PairDropGS directly constrains the low-frequency structural responses between paired dropped Gaussian subsets, which helps suppress dropout-induced instability and promotes more reliable scene structures. Consequently, both PairDropGS and PairDropGS-S recover cleaner geometry, sharper boundaries, and more faithful details across challenging regions, yielding better visual quality than existing dropout-based methods.

D. Stability Analysis

To evaluate the robustness of different dropout-based methods under training randomness, we conduct a stability analysis on two representative dropout-based methods, i.e., DropoutGS [18] and DropGaussian [19], together with our PairDropGS on the LLFF, Mip-NeRF360, and Blender datasets under challenging sparse-view settings. Following multi-seed evaluation protocols [20], [24], each method is independently trained 10 times using different random seeds while keeping all other settings unchanged. We report the mean and standard deviation of PSNR, SSIM, and LPIPS over all runs. The corresponding results of three datasets are summarized in Tab. IV and Tab. V, respectively.

As shown in Tab. IV and Tab. V, PairDropGS achieves both stronger reconstruction performance and better stability across random seeds. On LLFF, PairDropGS obtains the best average results with 20.91 dB PSNR, 0.739 SSIM, and 0.182 LPIPS. More importantly, PairDropGS substantially improves training stability by reducing the PSNR standard deviation from 0.1724 to 0.0726 compared with DropGaussian, indicating that the learned Gaussian representation becomes significantly less sensitive to dropout-induced inconsistency during training. A

TABLE V: Per-scene PSNR fluctuation on the Mip-NeRF360 dataset under 12-view settings and Blender dataset under 8-view settings. We report PSNR mean ± standard deviation over 10 random seeds.

Method	Mip-NeRF360							Average
	Bicycle	Bonsai	Counter	Garden	Kitchen	Room	Stump	
DropGaussian	19.64±0.217	19.00±0.204	18.39±0.217	20.46±0.174	20.50±0.220	20.62±0.191	17.03±0.280	19.38±0.114
PairDropGS	**20.39**±**0.053**	**19.84**±**0.176**	**19.02**±**0.133**	**20.85**±**0.094**	**21.20**±**0.126**	**21.21**±**0.087**	**18.25**±**0.102**	**20.11**±**0.040**

Method	Blender								Average
	Chair	Drums	Ficus	Hotdog	Lego	Material	Mic	Ship	
DropGaussian	25.85±0.051	21.87±0.050	26.39±0.112	25.94±0.105	23.85±0.143	22.91±0.177	29.55±0.196	25.11±0.094	25.18±0.116
PairDropGS	**26.26**±**0.057**	**21.85**±**0.039**	**26.75**±**0.079**	**26.69**±**0.064**	**24.66**±**0.093**	**22.77**±**0.104**	**29.79**±**0.090**	**25.82**±**0.076**	**25.57**±**0.024**

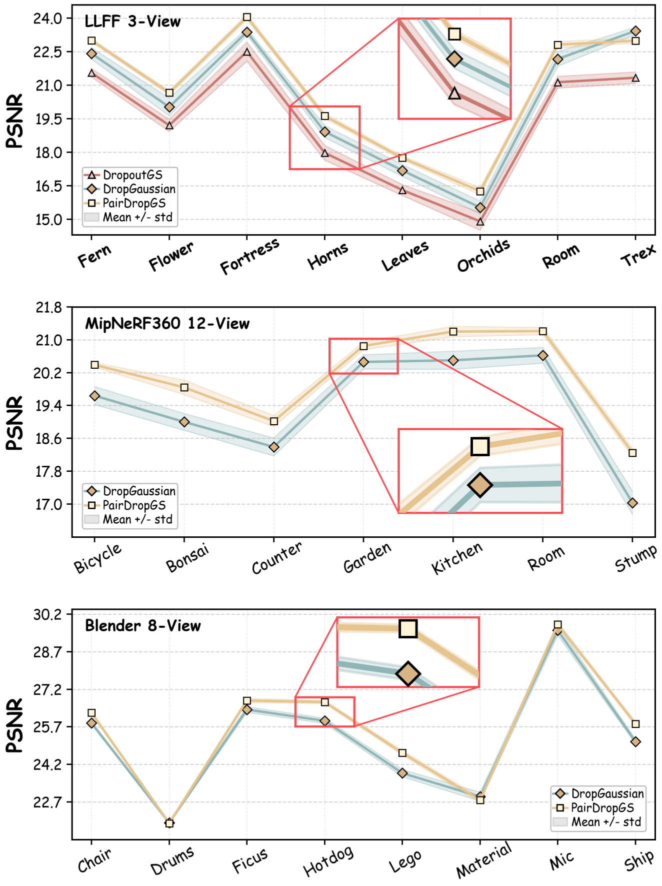

Fig. 7: Per-scene PSNR fluctuation of three datasets.

similar trend can also be observed in SSIM and LPIPS, where PairDropGS achieves both better average results and lower variance. Similar robustness improvements can also be consistently observed on the Mip-NeRF360 and Blender datasets, demonstrating that PairDropGS effectively stabilizes sparse-view Gaussian representation learning across different scenes and sparsity settings. These results validate the effectiveness of our paired consistency regularization design for robust sparse-view Gaussian splatting.

TABLE VI: Compatibility with existing sparse-view reconstruction methods on the LLFF dataset under 3-view settings.

Method	PSNR↑	SSIM↑	LPIPS↓	Avg. Time↓
FSGS [13]	20.43	0.682	0.248	276 s
FSGS + ***Ours***	**20.69**	**0.718**	**0.206**	406 s
FSGS + ***Ours-S***	20.58	0.713	0.221	**250** s
CoR-GS [14]	20.36	0.710	0.202	**373** s
CoR-GS + ***Ours***	**20.74**	**0.721**	**0.199**	514 s
CoR-GS + ***Ours-S***	20.58	0.716	0.200	376 s
DropGaussian [19]	20.33	0.709	0.201	74 s
DropGaussian + ***Ours***	**20.91**	**0.740**	**0.182**	134 s
DropGaussian + ***Ours-S***	20.70	0.729	0.191	**71** s

E. Compatibility

To further verify the generality of the proposed consistency regularization, we integrate our methods into several representative 3DGS-based works, including FSGS [13], CoR-GS [14], and DropGaussian [19].

For fair comparison, we keep the original training pipeline and baseline-specific settings unchanged, and only append our proposed paired consistency regularization to the training objective. Our two methods are adopted: ***Ours*** uses the original training schedule with the full PairDropGS integration, while ***Ours-S*** uses the shortened training schedule with the PairDropGS-S integration that reduces the training iterations to keep the average training time close to the corresponding baseline. All experiments are conducted under the same sparse-view setting, and the corresponding quantitative and qualitative results are reported in Tab. VI and Fig. 8, respectively.

As shown in Tab. VI, incorporating PairDropGS consistently improves the reconstruction performance of all compared baselines. In particular, the augmented variants achieve higher PSNR and SSIM together with lower LPIPS than their original counterparts, demonstrating that the proposed design is broadly compatible with different 3DGS-based frameworks. Moreover, the visual comparisons in Fig. 8 further show that our plug-in strategy suppresses unstable structures and produces cleaner and more reliable reconstructions in challenging sparse-view regions. Notably, the time-matched variant, i.e., ***Ours-S***, still preserves clear performance gains under comparable training cost, indicating that our PairDropGS framework can improve existing methods without introducing excessive

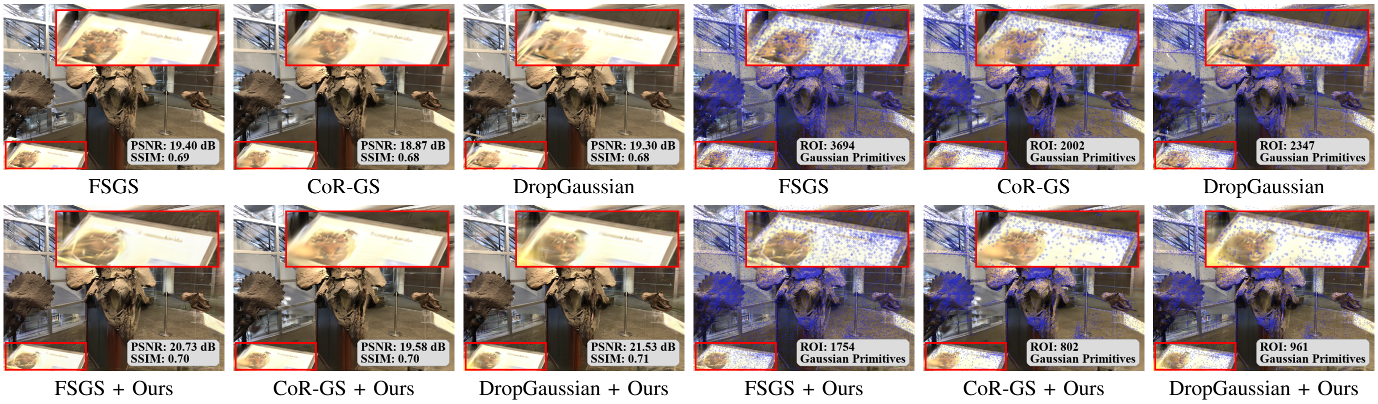

Fig. 8: Plug-and-play compatibility on the LLFF dataset under 3-view settings. PairDropGS can be easily integrated into different 3DGS variants and consistently improves reconstruction quality.

TABLE VII: Ablation study on the LLFF dataset under 3-view settings.

Two-branch Rec.	Low-freq. Cons.	Prog. Cons.	PSNR↑	SSIM↑	LPIPS↓	Avg. Time↓
×	×	×	20.34	0.711	0.201	74 s
✓	×	×	20.58	0.726	0.199	123 s
✓	✓	×	20.77	0.729	0.190	135 s
✓	✓	✓	**20.89**	**0.740**	**0.182**	134 s

computational overhead.

These results demonstrate that the proposed paired consistency regularization is not limited to a specific baseline architecture. By explicitly stabilizing the structural responses rendered from different dropped Gaussian subsets during training, PairDropGS can be seamlessly integrated into existing 3DGS variants to improve sparse-view reconstruction quality in a plug-and-play manner.

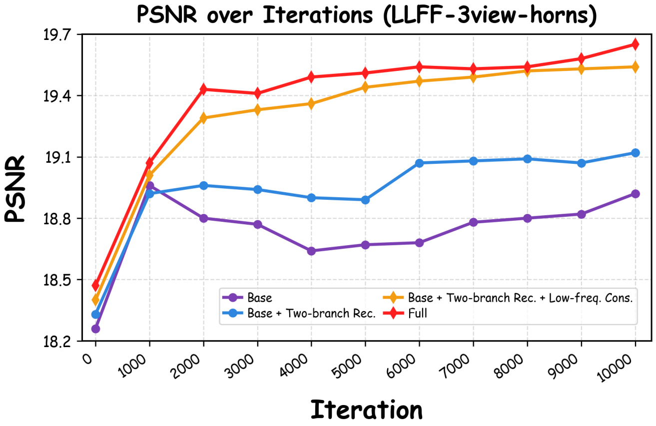

Fig. 9: Training PSNR curves of different ablation variants on the challenging LLFF 3-view *horns* scene. PairDropGS achieves more stable optimization and better convergence behavior throughout training.

F. Ablation Study

We conduct ablation experiments on the LLFF dataset under challenging 3-view settings to validate the effectiveness of each component in PairDropGS. All ablation studies are built upon the DropGaussian [19] baseline under the same training protocol. We report PSNR, SSIM, and LPIPS to evaluate reconstruction quality, and further analyze the training cost under different numbers of branches.

1) Effect of the Proposed Designs. In particular, besides the single-branch DropGaussian baseline, we further introduce a two-branch variant, i.e., *Two-branch Rec.*, that only uses two-branch reconstruction supervision. In this variant, two independently dropped Gaussian subsets are rendered in each iteration and supervised by the same ground-truth view, without applying the proposed low-frequency consistency loss. This setting allows us to distinguish the improvement brought by simple two-branch supervision from that brought by explicit consistency regularization. Starting from this variant, we further add low-frequency consistency i.e., *Low-freq. Cons.*, regularization and progressive consistency scheduling i.e., *Prog. Cons.*. For fair comparison, all variants are trained under the same setting, and only the corresponding component under study is changed. The results are reported in Tab. VII.

As shown in Tab. VII, introducing the two-branch reconstruction loss already improves the single-branch baseline, since two independently dropped Gaussian subsets are supervised within each iteration. However, this variant only benefits from additional branch supervision and does not explicitly stabilize the structural responses rendered from different dropped subsets. After adding the proposed low-frequency consistency regularization, the performance is further improved, demonstrating that the gain of PairDropGS cannot be attributed merely to two-branch supervision. Instead, explicitly constraining the low-frequency structural responses between paired dropped Gaussian subsets is important for learning more reliable scene structures under sparse supervision. Finally, the progressive consistency schedule brings additional improvements, indicating that gradually strengthening the consistency constraint is more effective than applying a fixed strong constraint throughout training. To further analyze the optimization behavior, we plot the training PSNR curves of different ablation variants on the LLFF 3-view *horns*

TABLE VIII: Effect of the different number of branches on the LLFF dataset under 3-view settings.

Model	Branch	PSNR↑	SSIM↑	LPIPS↓	Avg. Time↓
PairDropGS	1	20.34	0.711	0.201	74 s
	2	20.89	0.740	**0.182**	134 s
	3	**20.91**	**0.741**	0.183	191 s
PairDropGS-S	1	20.23	0.692	0.214	**41** s
	2	20.70	0.729	**0.191**	71 s
	3	**20.76**	**0.730**	0.192	101 s

scene in Fig. 9. Compared with the baseline, the two-branch reconstruction variant improves the PSNR throughout training. After adding low-frequency consistency regularization, the curve becomes consistently higher, indicating that constraining low-frequency structural responses helps stabilize sparse-view optimization. Moreover, the full PairDropGS achieves the best convergence behavior, especially during later optimization, which supports the effectiveness of the progressive consistency scheduling.

Overall, these results validate that PairDropGS benefits from both low-frequency consistency regularization and stage-aware progressive weight scheduling, beyond the effect of simple two-branch supervision.

2) Effect of the Number of Branches. We further study the trade-off between reconstruction performance and computational cost when increasing the number of dropped Gaussian subset branches. Starting from the single-branch DropGaussian baseline, we compare the default two-branch PairDropGS with a three-branch extension. For fair comparison, all variants are built upon the same baseline and trained under the same setting. In addition to reconstruction metrics, we also report the average training time. The results are shown in Tab. VIII. For the three-branch extension, three dropped Gaussian subsets are obtained from the same shared Gaussian field during each iteration. Each branch is supervised by the same ground-truth view, and low-frequency consistency regularization is applied between every pair of rendered branches. Specifically, three pairwise consistency constraints are introduced while all other settings remain unchanged.

As shown in Tab. VIII, moving from one branch to two branches yields substantial performance improvements, confirming the effectiveness of constraining the structural responses rendered from paired dropped Gaussian subsets. Although the two-branch design increases the training time compared with the single-branch baseline, it brings clear reconstruction gains. By contrast, further increasing the number of branches from two to three only brings marginal improvements, while introducing much higher computational cost. For example, in the full setting, the PSNR only increases from 20.89 to 20.91 when using three branches, but the average training time increases from 134 s to 191 s. A similar trend can also be observed in the lightweight PairDropGS-S setting, where increasing the number of branches from two to three only improves PSNR by 0.06 dB while introducing an additional 30 s training cost. These results indicate that the two-branch formulation provides a favorable balance between reconstruction quality and efficiency. Therefore, we adopt the two-branch design as the default setting of PairDropGS.

VI. CONCLUSION

In this paper, we propose **PairDropGS**, a simple yet effective **Pair**ed **Drop**out-induced Consistency Regularization framework for sparse-view 3D **G**aussian **S**platting. Different from existing dropout-based methods that mainly focus on increasingly sophisticated dropout strategies, PairDropGS improves sparse-view reconstruction by explicitly stabilizing the structural responses rendered from different dropped Gaussian subsets during training. Specifically, we introduce paired branch optimization, low-frequency consistency regularization, and progressive consistency scheduling to improve the stability and robustness of dropout-based optimization under sparse-view supervision. Extensive experiments on multiple sparse-view benchmarks demonstrate that PairDropGS significantly and consistently improves training stability, reconstruction quality and robustness over existing dropout-based methods while preserving the simplicity and plug-and-play nature for improving dropout-based optimization. We believe this work provides a new perspective for analyzing and enhancing dropout-based sparse-view Gaussian optimization, and may serve as a strong and generalizable baseline for future sparse-view Gaussian splatting research.

REFERENCES

[1] B. Kerbl, G. Kopanas, T. Leimkühler, and G. Drettakis, “3d gaussian splatting for real-time radiance field rendering,” *ACM Trans. Graph.*, vol. 42, no. 4, pp. 1–14, 2023.

[2] G. Chen and W. Wang, “A survey on 3d gaussian splatting,” arXiv:2401.03890, 2024.

[3] B. Fei, J. Xu, R. Zhang, Q. Zhou, W. Yang, and Y. He, “3d gaussian splatting as new era: A survey,” *IEEE Trans. Vis. Comput. Graph.*, 2024.

[4] Z. Yu, A. Chen, B. Huang, T. Sattler, and A. Geiger, “Mip-splatting: Alias-free 3d gaussian splatting,” in *Proc. IEEE/CVF Conf. Comput. Vis. Pattern Recognit.*, 2024, pp. 19 447–19 456.

[5] Y. Jiang, J. Tu, Y. Liu, X. Gao, X. Long, W. Wang, and Y. Ma, “Gaussianshader: 3d gaussian splatting with shading functions for reflective surfaces,” in *Proc. IEEE/CVF Conf. Comput. Vis. Pattern Recognit.*, 2024, pp. 5322–5332.

[6] J. T. Barron, B. Mildenhall, M. Tancik, P. Hedman, R. Martin-Brualla, and P. P. Srinivasan, “Mip-nerf: A multiscale representation for anti-aliasing neural radiance fields,” in *Proc. IEEE/CVF Int. Conf. Comput. Vis.*, 2021, pp. 5855–5864.

[7] J. T. Barron, B. Mildenhall, D. Verbin, P. P. Srinivasan, and P. Hedman, “Mip-nerf 360: Unbounded anti-aliased neural radiance fields,” in *Proc. IEEE/CVF Conf. Comput. Vis. Pattern Recognit.*, 2022, pp. 5470–5479.

[8] M. Niemeyer, J. T. Barron, B. Mildenhall, M. S. M. Sajjadi, A. Geiger, and N. Radwan, “Regnerf: Regularizing neural radiance fields for view synthesis from sparse inputs,” in *Proc. IEEE/CVF Conf. Comput. Vis. Pattern Recognit.*, 2022, pp. 5480–5490.

[9] T. Müller, A. Evans, C. Schied, and A. Keller, “Instant neural graphics primitives with a multiresolution hash encoding,” *ACM Trans. Graph.*, vol. 41, no. 4, pp. 102:1–102:15, 2022.

[10] J. Yang, M. Pavone, and Y. Wang, “Freenerf: Improving few-shot neural rendering with free frequency regularization,” in *Proc. IEEE/CVF Conf. Comput. Vis. Pattern Recognit.*, 2023, pp. 8254–8263.

[11] G. Wang, Z. Chen, C. C. Loy, and Z. Liu, “Sparsenerf: Distilling depth ranking for few-shot novel view synthesis,” in *Proc. IEEE/CVF Int. Conf. Comput. Vis.*, 2023, pp. 9065–9076.

[12] J. Li, J. Zhang, X. Bai, J. Zheng, X. Ning, J. Zhou, and L. Gu, “Dngaussian: Optimizing sparse-view 3d gaussian radiance fields with global-local depth normalization,” in *Proc. IEEE/CVF Conf. Comput. Vis. Pattern Recognit.*, 2024, pp. 20 775–20 785.

[13] Z. Zhu, Z. Fan, Y. Jiang, and Z. Wang, “Fsgs: Real-time few-shot view synthesis using gaussian splatting,” in *Eur. Conf. Comput. Vis.*, 2024, pp. 145–163.

[14] J. Zhang, J. Li, X. Yu, L. Huang, L. Gu, J. Zheng, and X. Bai, “Cor-gs: Sparse-view 3d gaussian splatting via co-regularization,” in *Eur. Conf. Comput. Vis.*, 2024, pp. 335–352.

[15] Y. Zheng, Z. Jiang, S. He, Y. Sun, J. Dong, H. Zhang, and Y. Du, “Nexusgs: Sparse view synthesis with epipolar depth priors in 3d gaussian splatting,” in *Proc. IEEE/CVF Conf. Comput. Vis. Pattern Recognit.*, 2025, pp. 26 800–26 809.

[16] H. Nguyen, R. Li, A. Le, and T. Nguyen, “Dwtgs: Rethinking frequency regularization for sparse-view 3d gaussian splatting,” arXiv:2507.15690, 2025.

[17] C. Zhao, X. Wang, T. Zhang, and et al., “Self-ensembling gaussian splatting for few-shot novel view synthesis,” in *Proc. IEEE/CVF Int. Conf. Comput. Vis.*, 2025, pp. 4940–4950.

[18] Y. Xu, L. Wang, M. Chen, S. Ao, L. Li, and Y. Guo, “Dropoutgs: Dropping out gaussians for better sparse-view rendering,” in *Proc. IEEE/CVF Conf. Comput. Vis. Pattern Recognit.*, 2025, pp. 701–710.

[19] H. Park, G. Ryu, and W. Kim, “Dropgaussian: Structural regularization for sparse-view gaussian splatting,” in *Proc. IEEE/CVF Conf. Comput. Vis. Pattern Recognit.*, 2025, pp. 21 600–21 609.

[20] M. Song, X. Lin, D. Zhang, H. Li, X. Li, B. Du, and L. Qi, “d^2gs: Depth-and-density guided gaussian splatting for stable and accurate sparse-view reconstruction,” arXiv:2510.08566, 2025.

[21] H. Li, Q. Zhu, X. Meng, D. Zhao, and X. Fan, “Doc-gs: Dual-domain observation and calibration for reliable sparse-view gaussian splatting,” arXiv:2604.06739, 2026.

[22] S. Fang, I.-C. Shen, X. Zhang, Z. Wang, Y. Wang, W. Ding, G. Yu, and T. Igarashi, “Dropping anchor and spherical harmonics for sparse-view gaussian splatting,” arXiv:2602.20933, 2026.

[23] Z. Guo, P. Wang, Z. Chen *et al.*, “Ugod: Uncertainty-guided differentiable opacity and soft dropout for enhanced sparse-view 3dgs,” *arXiv preprint arXiv:2508.04968*, 2025.

[24] K. Chen, Y. Zhong, Z. Li, J. Lin, Y. Chen, M. Qin, and H. Wang, “Quantifying and alleviating co-adaptation in sparse-view 3d gaussian splatting,” arXiv:2508.12720, 2025.

[25] B. Mildenhall, P. P. Srinivasan, M. Tancik, J. T. Barron, R. Ramamoorthi, and R. Ng, “Nerf: Representing scenes as neural radiance fields for view synthesis,” in *Eur. Conf. Comput. Vis.*, 2020, pp. 405–421.

[26] H. Fu, X. Yu, L. Li, Y. Zhang, and J. Wang, “Cbarf: Cascaded bundle-adjusting neural radiance fields from imperfect camera poses,” *IEEE Trans. Multimedia*, vol. 26, pp. 9304–9315, 2024.

[27] Y. Chen, L. Zhang, S. Zhao, X. Liu, and H. Wang, “Atm-nerf: Accelerating training for nerf rendering on mobile devices via geometric regularization,” *IEEE Trans. Multimedia*, vol. 27, pp. 3279–3293, 2025.

[28] K. Guo, Z. Wu, X. Wen, Y. Liu, and H. Chen, “Gan prior-enhanced novel view synthesis from monocular degraded images,” *IEEE Trans. Multimedia*, 2025.

[29] A. Yu, V. Ye, M. Tancik, and A. Kanazawa, “pixelNeRF: Neural radiance fields from one or few images,” in *Proc. IEEE/CVF Conf. Comput. Vis. Pattern Recognit.*, 2021, pp. 4578–4587.

[30] Q. Wang, Z. Wang, K. Genova, P. Srinivasan, H. Zhou, J. T. Barron, R. Martin-Brualla, N. Snavely, and T. Funkhouser, “IBRNet: Learning multi-view image-based rendering,” in *Proc. IEEE/CVF Conf. Comput. Vis. Pattern Recognit.*, 2021, pp. 4690–4699.

[31] A. Chen, Z. Xu, F. Zhao, X. Zhang, F. Xiang, J. Yu, and H. Su, “MVSNeRF: Fast generalizable radiance field reconstruction from multi-view stereo,” in *Proc. IEEE/CVF Int. Conf. Comput. Vis.*, 2021, pp. 14 124–14 133.

[32] Z. Yu, A. Chen, B. Huang, T. Sattler, and A. Geiger, “Mip-splatting: Alias-free 3d gaussian splatting,” in *Proc. IEEE/CVF Conf. Comput. Vis. Pattern Recognit.*, 2024, pp. 19 447–19 456.

[33] T. Lu, M. Yu, L. Xu, Y. Xiangli, L. Wang, D. Lin, and B. Dai, “Scaffold-gs: Structured 3d gaussians for view-adaptive rendering,” in *Proc. IEEE/CVF Conf. Comput. Vis. Pattern Recognit.*, 2024, pp. 20 654–20 664.

[34] K. Cheng, X. Long, K. Yang, Y. Yao, W. Yin, Y. Ma, W. Wang, and X. Chen, “Gaussianpro: 3d gaussian splatting with progressive propagation,” in *Proc. 41st Int. Conf. Mach. Learn.*, 2024.

[35] Z. Huang, M. Xu, and S. Perry, “Structgs: Adaptive spherical harmonics and rendering enhancements for superior 3d gaussian splatting,” *IEEE Trans. Multimedia*, 2025.

[36] Y. Zhao, G. Chen, B. Wu, Y. Li, and H. Zhang, “Msa-splatting: Multi-scale adaptive gaussian splatting for high-fidelity view synthesis,” *IEEE Trans. Multimedia*, 2026.

[37] Y. Chen, H. Xu, C. Zheng, B. Zhuang, M. Pollefeys, A. Geiger, T.-J. Cham, and J. Cai, “MVSplat: Efficient 3D gaussian splatting from sparse multi-view images,” in *Proc. Eur. Conf. Comput. Vis.*, 2024, pp. 370–386.

[38] J. Chung, J. Oh, and K. M. Lee, “Depth-regularized optimization for 3D gaussian splatting in few-shot images,” in *Proc. IEEE/CVF Conf. Comput. Vis. Pattern Recognit.*, 2024, pp. 811–820.

[39] H. Xiong, S. Muttukuru, R. Upadhyay, P. Chari, and A. Kadambi, “SparseGS: Real-time 360° sparse view synthesis using gaussian splatting,” *arXiv preprint arXiv:2312.00206*, 2023.

[40] H. Kong, X. Liu, X. Chen, M. Di, Z. Wang, Z. Wu, B. Zhou, and D. Chen, “Generative sparse-view gaussian splatting,” in *Proc. IEEE/CVF Conf. Comput. Vis. Pattern Recognit.*, 2025.

[41] A. Jain, M. Tancik, and P. Abbeel, “Putting nerf on a diet: Semantically consistent few-shot view synthesis,” in *Proc. IEEE/CVF Int. Conf. Comput. Vis.*, 2021, pp. 5885–5894.

[42] B. Mildenhall, P. P. Srinivasan, R. Ortiz-Cayon, N. K. Kalantari, R. Ramamoorthi, R. Ng, and A. Kar, “Local light field fusion: Practical view synthesis with prescriptive sampling guidelines,” *ACM Trans. Graph.*, vol. 38, no. 4, pp. 1–14, 2019.